Electronic Supplementary Material

D-penicillamine-coated Cu/Ag alloy nanoclusters superstructure: aggregation-induced emission and tunable photoluminescence from red to orange

Lingcan Kong,*[a] Xuefeng Chu,[b] Chuanxi Wang,[c] Hong Zhou,[a] Yukang Wu[a] and Wenwei Liu*[a]

[a]*Wuxi Center for Disease Control and Prevention, Wuxi 214023, P. R. China;*
[b]*Jilin provincial key laboratory of architectural electricity & comprehensive energy saving, School of Electrical and Electronic Information Engineering, Jilin Jianzhu University, Changchun 130118, P. R. China;*
[c]*Institute of New Energy Technology, Ningbo Institute of Industrial Technology, Chinese Academy of Sciences, Ningbo 315201, P. R. China.*

Email: konglingcan2010@163.com; liuwwcdc@126.com

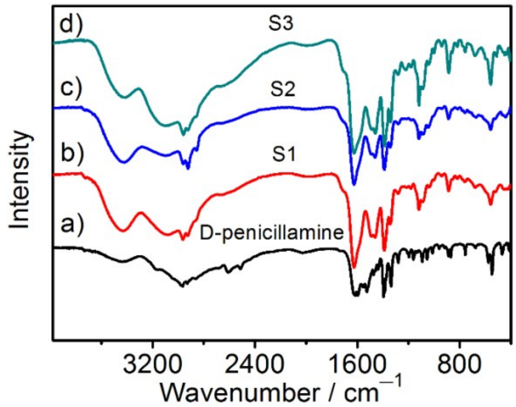

Figure S1 The FT-IR spectra of pure D-penicillamine (a), S1 (b), S2 (c), and S3 (d).

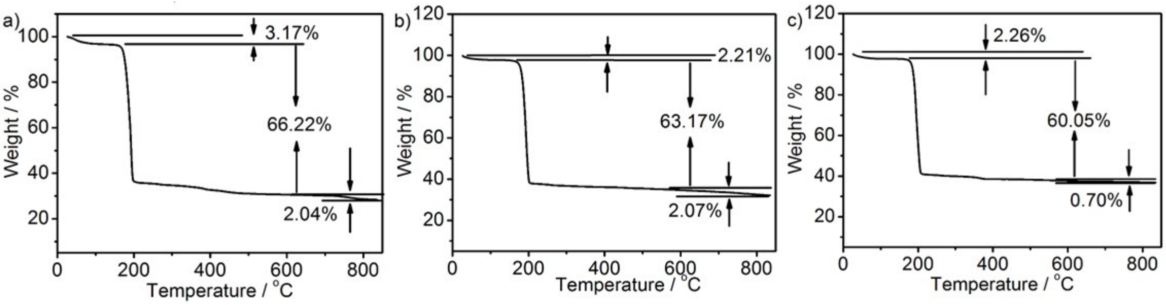

Figure S2 TGA thermograms of S1–S3 with the heating rate of 10°C/min, in which S1–S3 are (a), (b), (c), respectively.

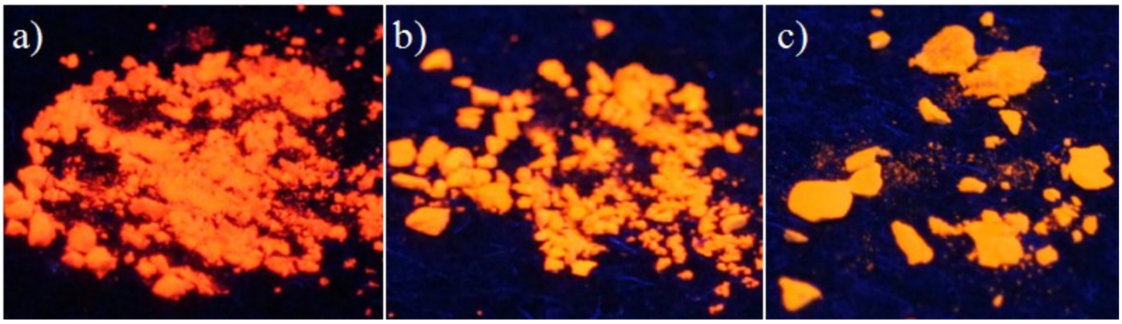

Figure S3 The powder of S1–S3 under a UV light with an excitation wavelength at 365 nm, in which S1–S3 are shown in (a), (b), (c), respectively.

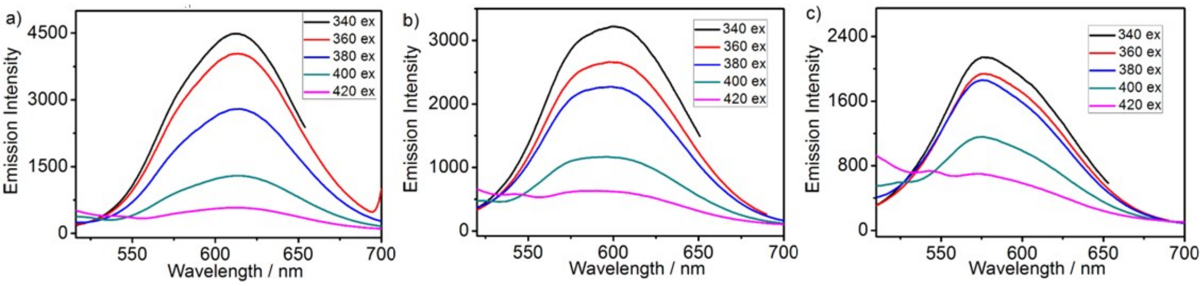

Figure S4 The emission spectra of S1–S3 by using different excitation wavelengths (340, 360, 380, 400, 420 nm), in which S1–S3 are shown in (a), (b), (c), respectively.

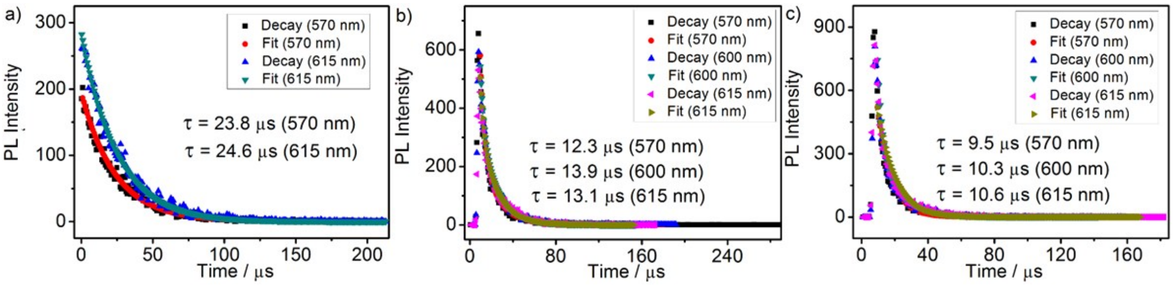

Figure S5 PL decay profiles of S1–S3 with the excitation of 355 nm and fitted curves are overlaid on the experimental data, in which S1–S3 are (a), (b), (c), respectively.

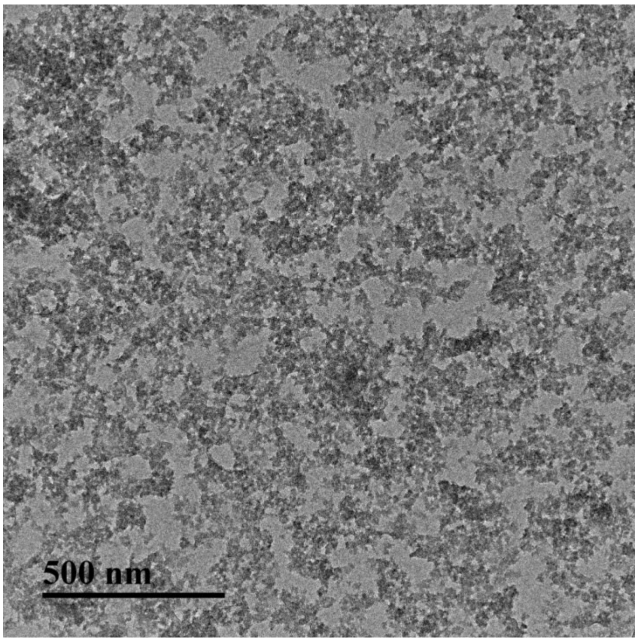

Figure S6 TEM image of S1.

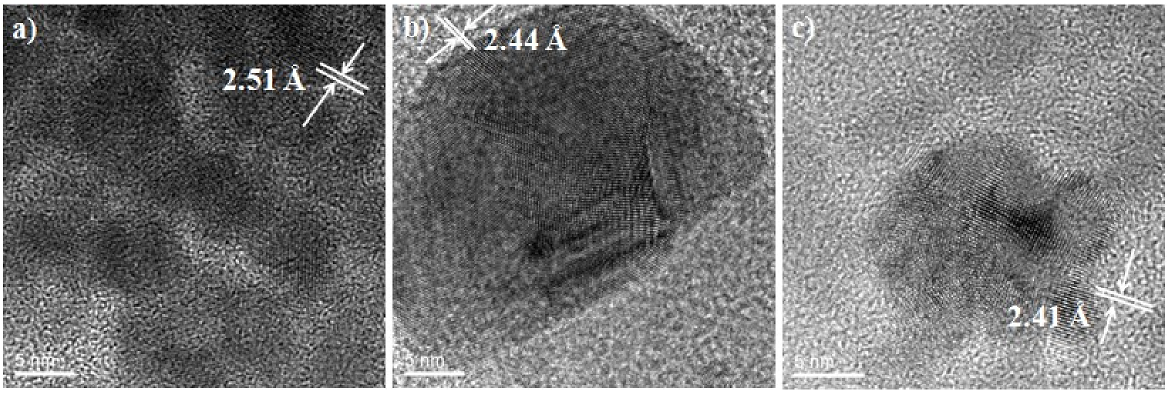

Figure S7 Crystal-lattice images of S1 (a), S2 (b), S3 (c). The scale bar is 5 nm.

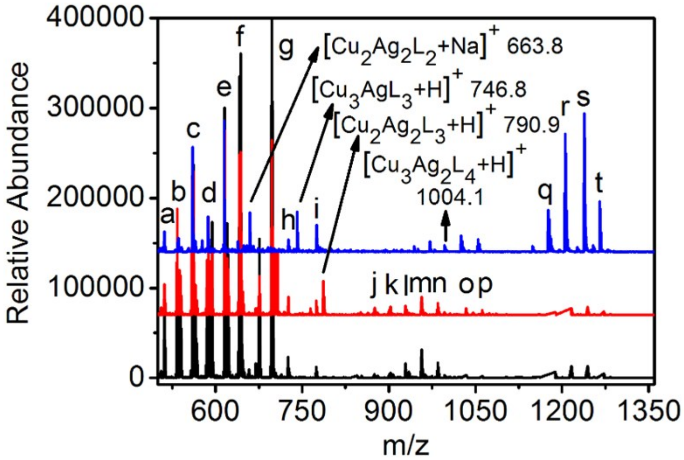

Figure S8 The ESI-TOF-mass data of S1 (black line), S2 (red line), and S3 (blue line) in methanol. The assignments of peaks are as following: a) $[Cu_3L_2+Na]^+$, 511.4; b) $[Cu_3L_2+2Na–H]^+$, 533.5; c) $[Cu_3L_2+CH_3OH+2Na–H]^+$, 565.4; d) $[Cu_4L_2+CH_3OH+H]^+$, 585.1; e) $[Cu_4L_2+2CH_3OH+H]^+$, 617.2; f) $[Cu_3L_3+H]^+$, 639.1; g) $[Cu_4L_3+H]^+$, 702.1; h) $[Cu_4L_3+Na]^+$, 724.4; i) $[Cu_4L_3+CH_3OH+2Na–H]^+$,778.6; j) $[Cu_4L_4+Na]^+$, 873.8; k) $[Cu_4L_4+CH_3OH+Na]^+$, 905.6; l) $[Cu_4L_4+CH_3OH+2Na–H]^+$, 927.7; m) $[Cu_5L_4+2Na–H]^+$, 958.9; n) $[Cu_5L_4++CH_3OH+2Na–H]^+$, 990.9; o) $[Cu_4L_5+CH_3OH+H]^+$, 1033.1; p) $[Cu_5L_5+H]^+$, 1064.1; q) $[Cu_7L_5+H]^+$, 1191.1; r) $[Cu_7L_5+Na]^+$, 1213.2; s) $[Cu_7L_5+CH_3OH+Na]^+$, 1245.2; t) $[Cu_6L_6+H]^+$, 1276.8.

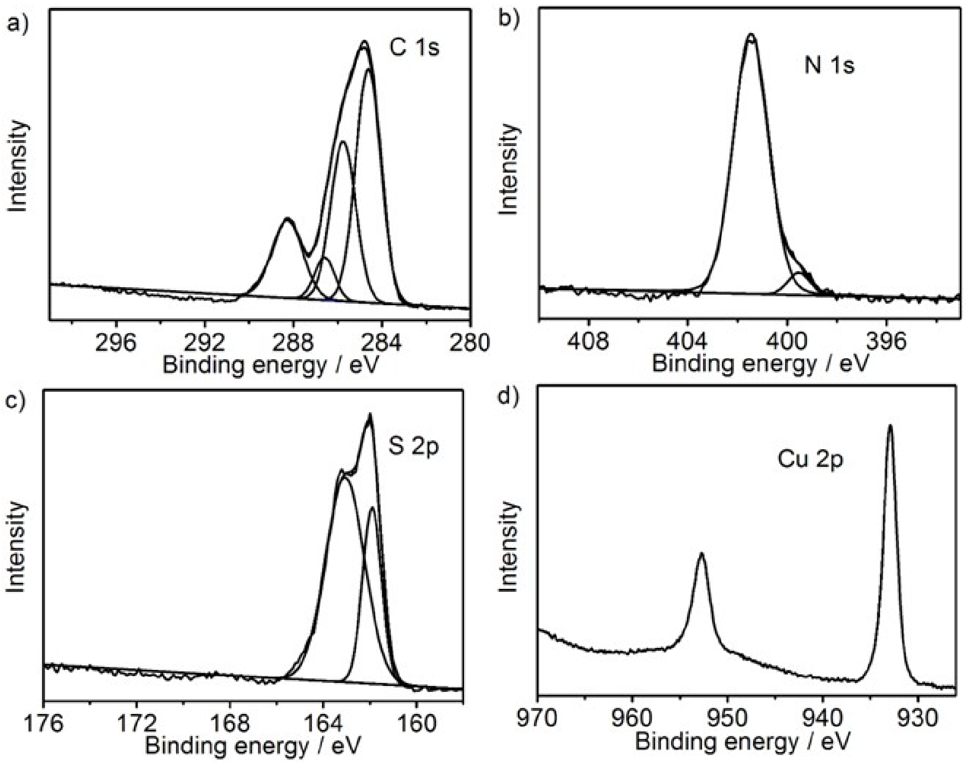

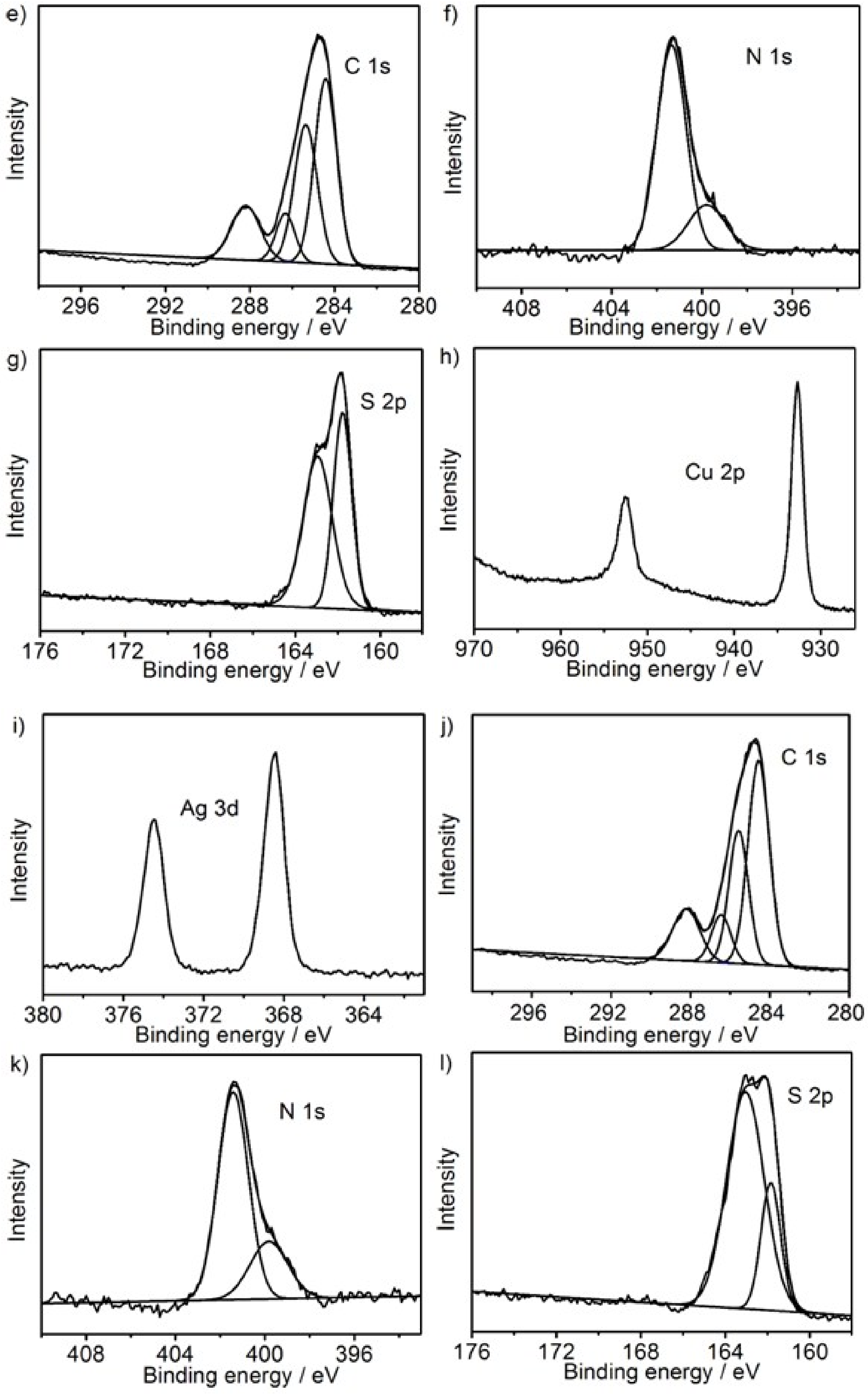
e)
C 1s
Intensity
296
292
288
284
280
Binding energy / eV
f)
N 1s
Intensity
408
404
400
396
Binding energy / eV
g)
S 2p
Intensity
176
172
168
164
160
Binding energy / eV
h)
Cu 2p
Intensity
970
960
950
940
930
Binding energy / eV
i)
Ag 3d
Intensity
380
376
372
368
364
Binding energy / eV
j)
C 1s
Intensity
296
292
288
284
280
Binding energy / eV
k)
N 1s
Intensity
408
404
400
396
Binding energy / eV
l)
S 2p
Intensity
176
172
168
164
160
Binding energy / eV

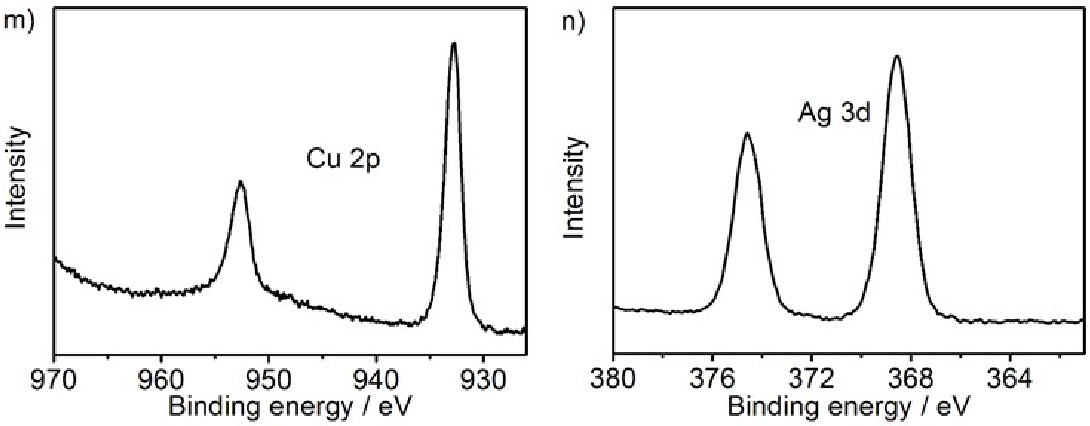

Figure S9 XPS spectra of S1–S3, in which C 1s, N 1s, S 2p, Cu 2p of S1 are shown in (a), (b), (c), (d); C 1s, N 1s, S 2p, Cu 2p, Ag 3d of S2 are shown in (e), (f), (g), (h), (i); C 1s, N 1s, S 2p, Cu 2p, Ag 3d of S3 are shown in (j), (k), (l), (m), (n), respectively.

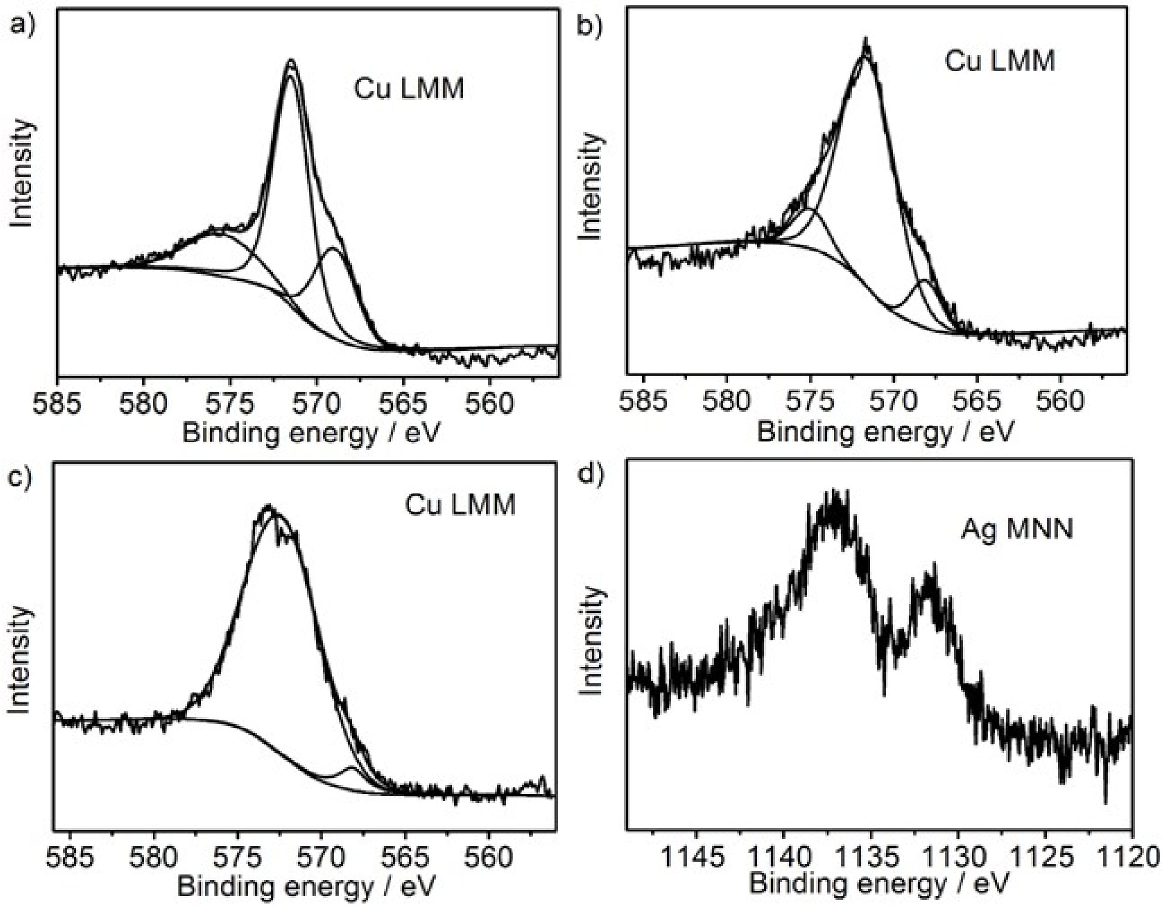

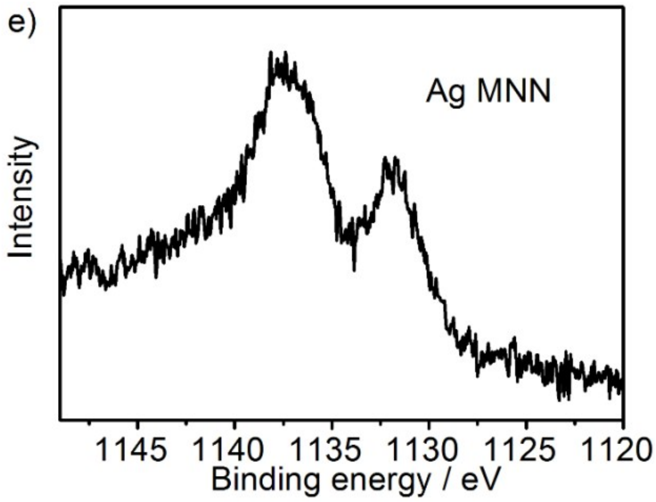

Figure S10 Auger electron spectra (AES) of S1–S3, in which Cu LMM AES of S1–S3 is shown in (a), (b), (c), respectively and AgMNN AES of S2 and S3 is shown in (d) and (e), respectively.

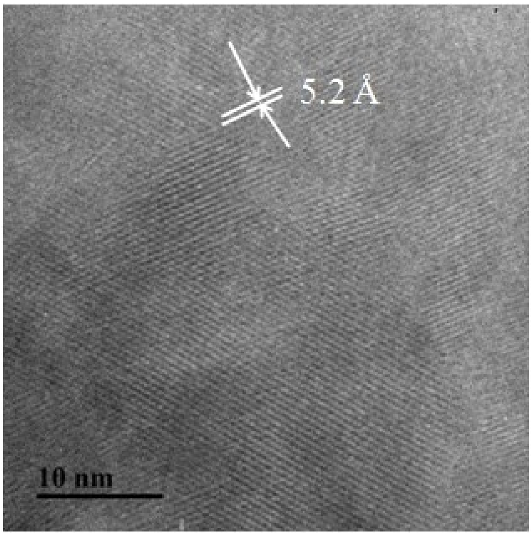

Figure S11 Crystal-lattice distance of S3 in high-resolution TEM.

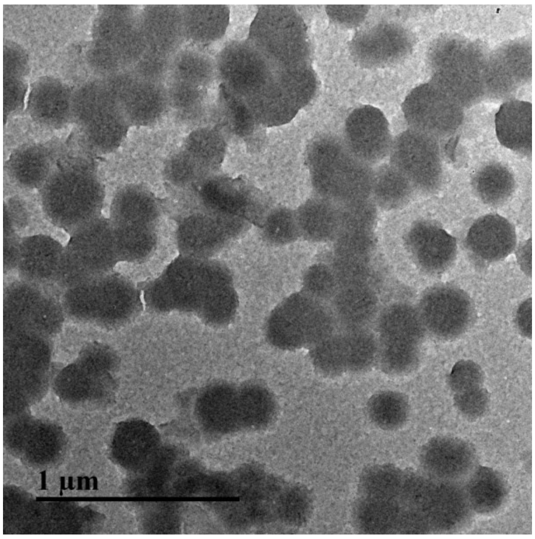

Figure S12 TEM image of S4.

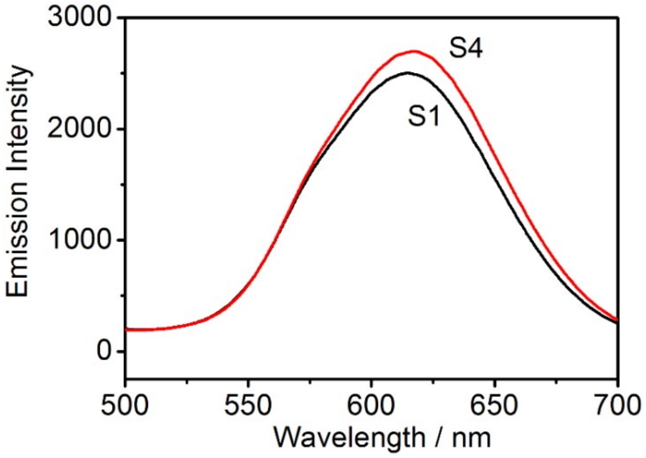

Figure S13 The emission spectra of S1 and S4 in aqueous solution.

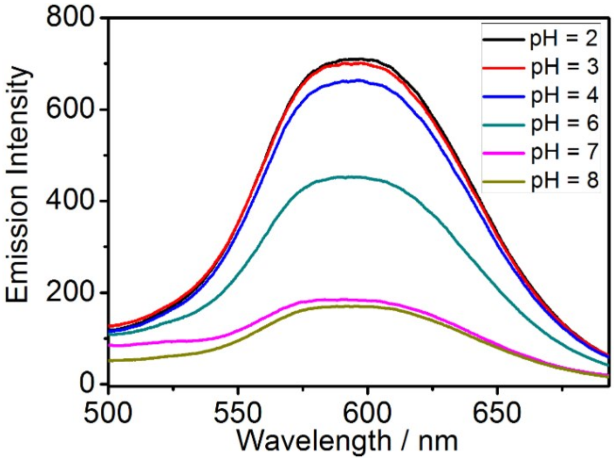

Figure S14 The emission intensity changes of S2 with the increase of pH value.

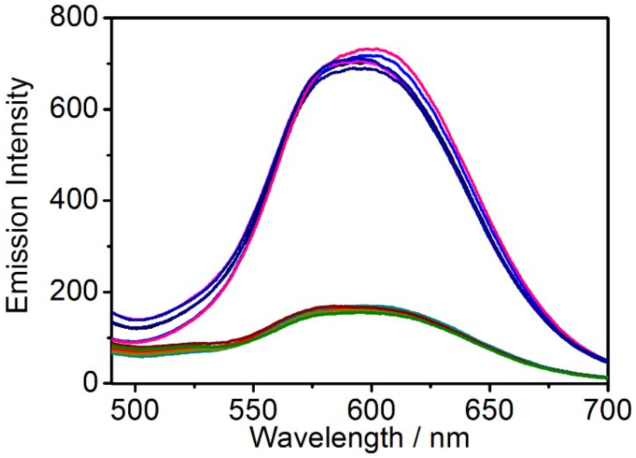

Figure S15 The emission intensity changes of S2 upon pH cycling between pH = 3 and 7.

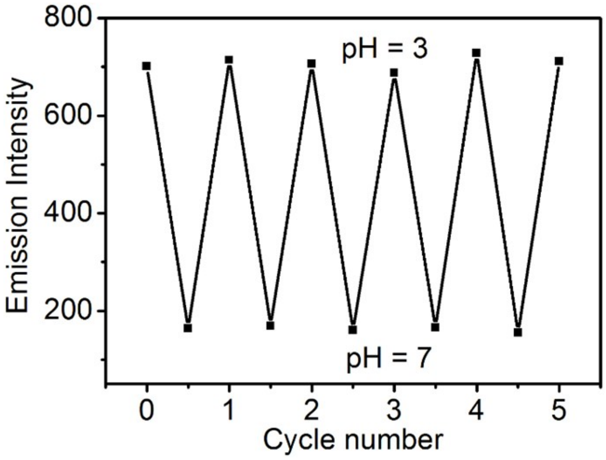

Figure S16 The emission intensity changes of S2 at 600 nm upon five numbers of pH cycling between pH = 3 and 7.

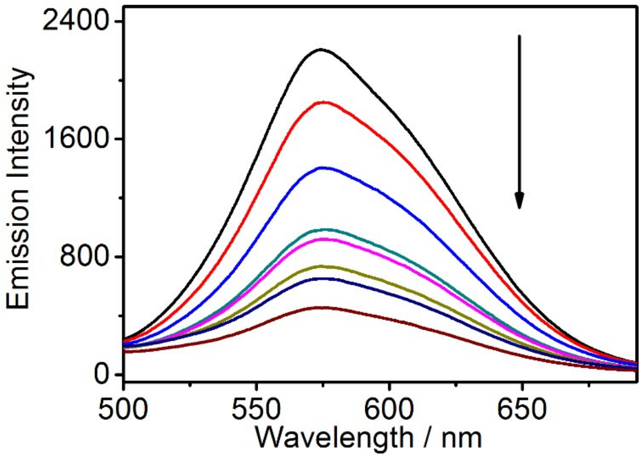

Figure S17 The emission intensity changes of S2 upon the increase of the temperature (5°C, 15°C, 30°C, 40°C, 48°C, 50°C, 60°C, 70°C).

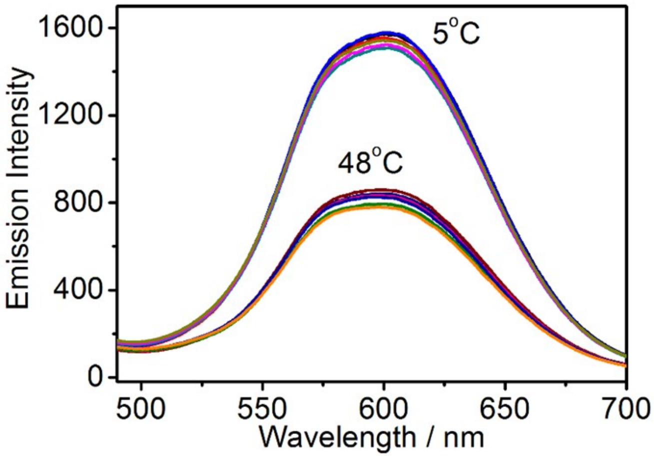

Figure S18 The emission intensity changes of S2 upon temperature cycling between 5°C and 48°C.

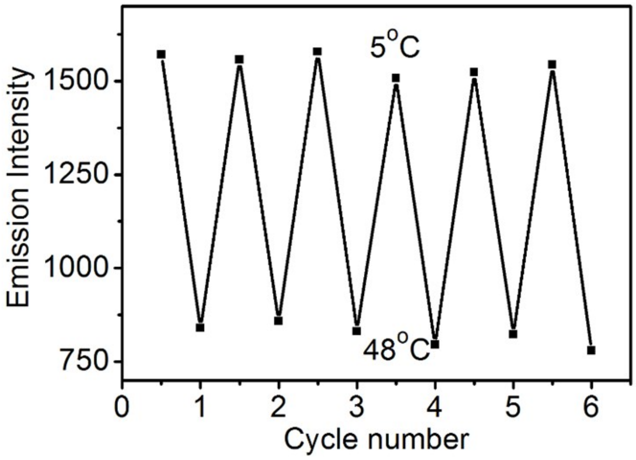

Figure S19 The emission intensity changes of S2 upon six numbers of temperature cycling between 5^{o}C and 48^{o}C.

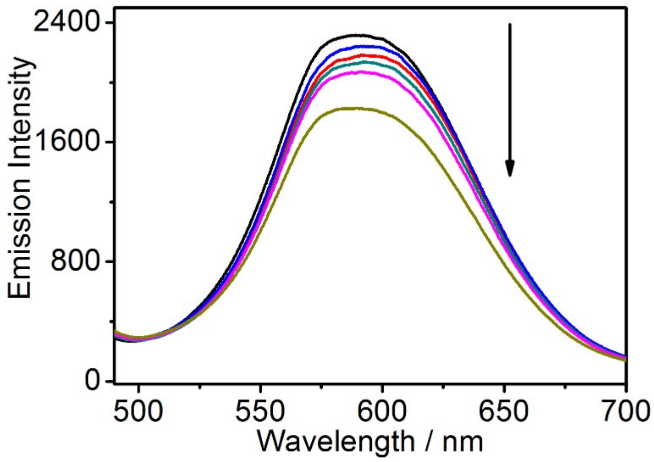

Figure S20 The emission intensity changes of S2 upon the increase of the amounts of D-penicillamine (3.5, 7, 10, 27, 40, 60 mg).

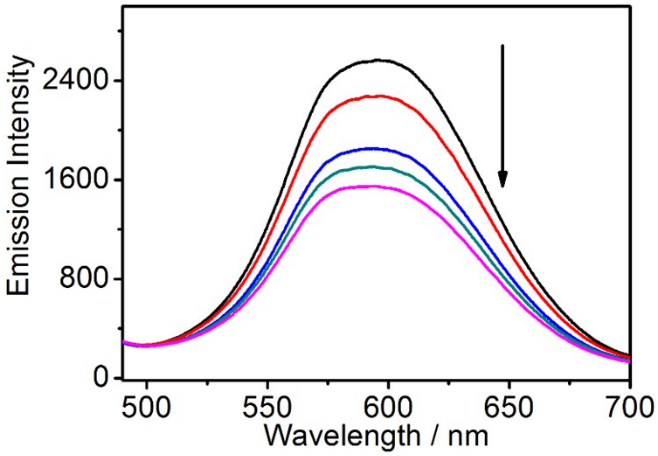

Figure S21 The emission intensity changes of S2 upon the increase of reaction time (0.5, 1, 1.5, 2, 2.5 h).

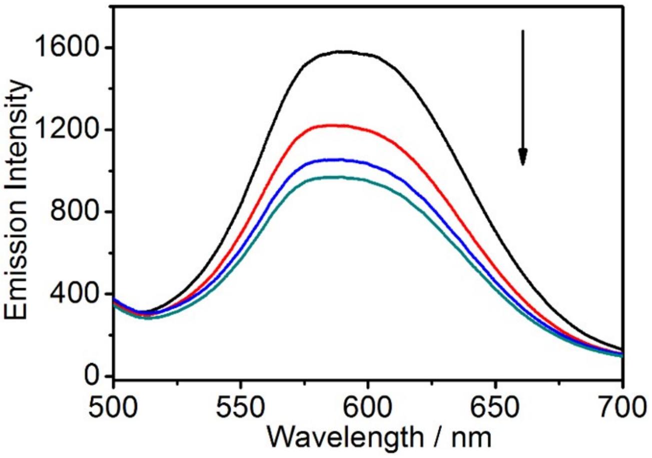

Figure S22 The emission intensity changes of S2 upon the increase of reaction temperature (20^{o}C, 40^{o}C, 60^{o}C, 80^{o}C).

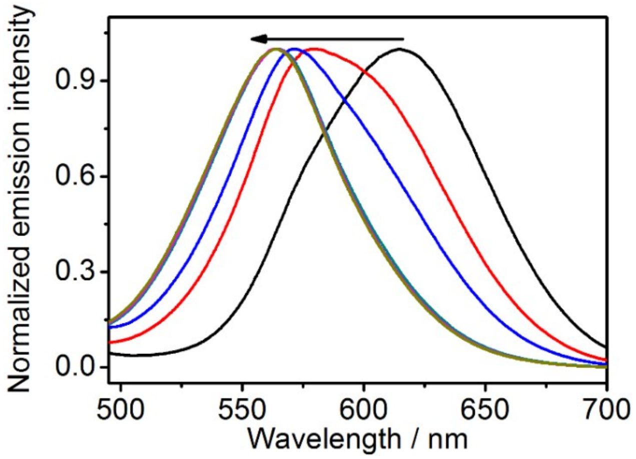

Figure S23 Normalized emission intensity of Cu/Ag nanoclusters with the increase of feed volume of $AgNO_3$ from 0 to 160 μL (0, 20, 40, 80, 120, 160 μL).

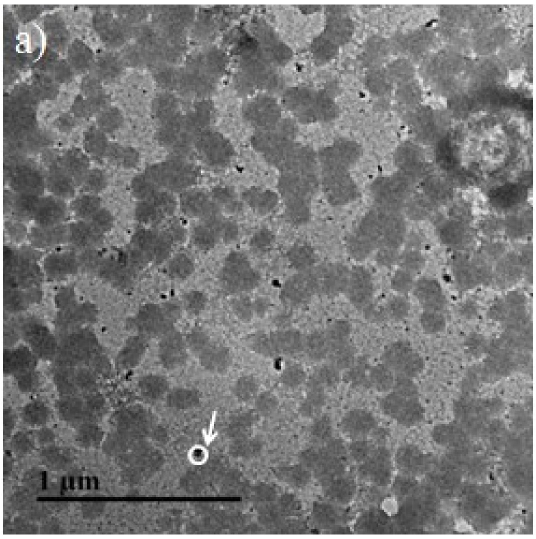

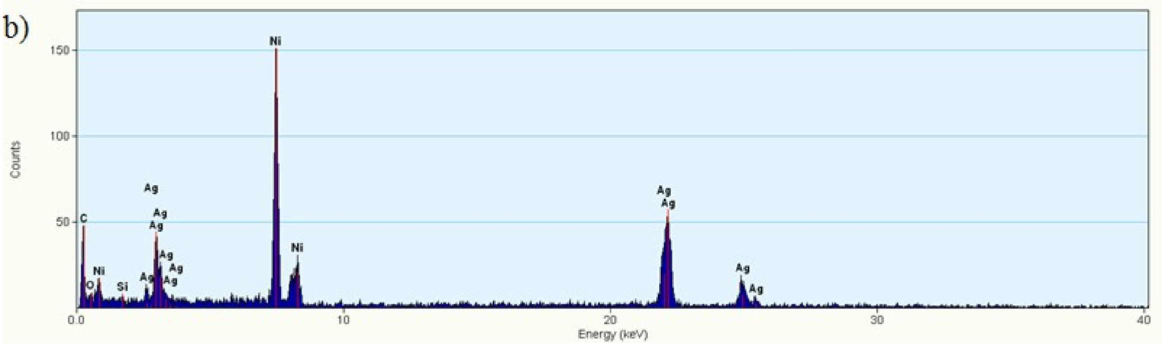

Figure S24 (a) TEM image of S5 and (b) EDX spectrum of the marked black dot in (a).

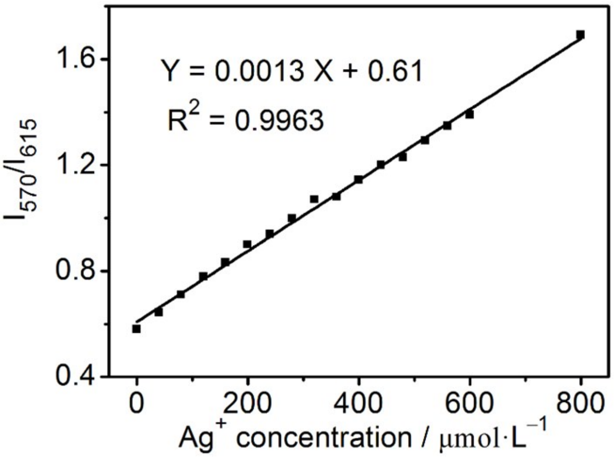

Figure S25 The linear relationship between the ratio of emission intensity of 570 and 615 nm (I_{570}/I_{615}) and the concentration of silver ion (0, 40, 80, 120, 160, 200, 240, 280, 320, 360, 400, 440, 480, 520, 560, 600, 800 μmol·L^{-1}).

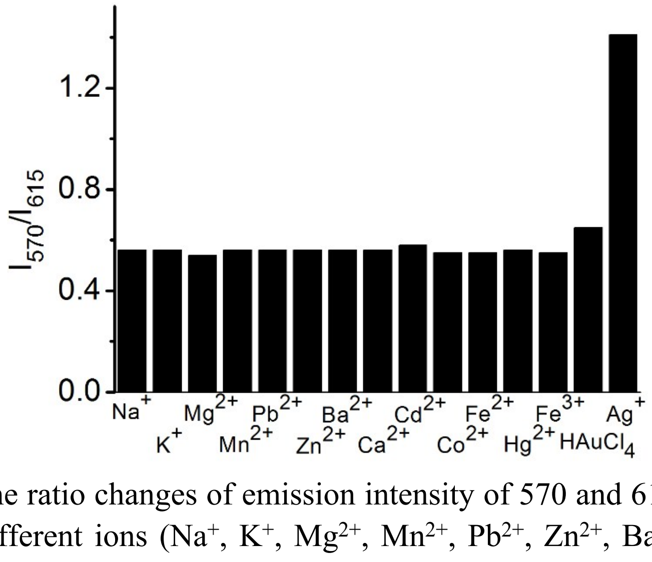

Figure S26 The ratio changes of emission intensity of 570 and 615 nm (I_{570}/I_{615}) upon addition of different ions (Na^+, K^+, Mg^{2+}, Mn^{2+}, Pb^{2+}, Zn^{2+}, Ba^{2+}, Ca^{2+}, Cd^{2+}, Co^{2+}, Fe^{2+}, Hg^{2+}, Fe^{3+}) and $HAuCl_4$ reacted with Cu(II) ion in the presence of D-penicillamine.

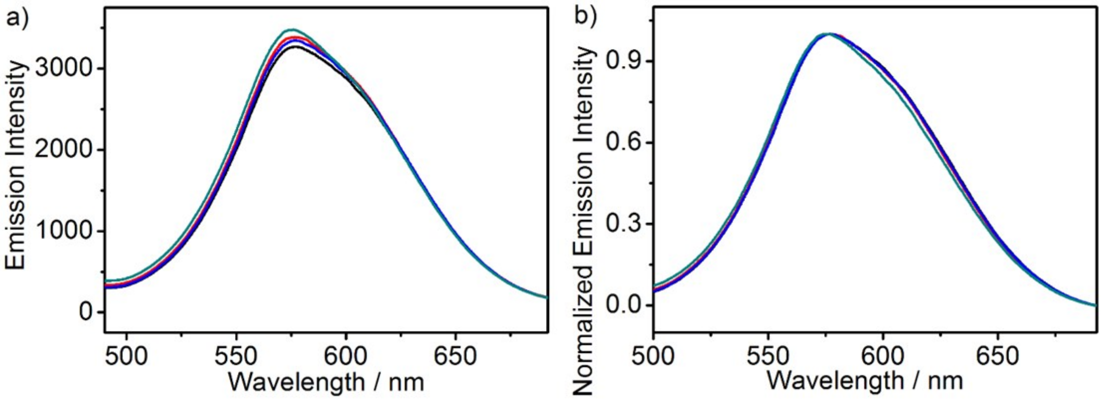

Figure S27 (a) The emission spectra and (b) normalized emission spectra of S3 prepared in tap water (black line), mineral water (red line), Tai lake water (blue line) and doubly distilled water (green line).

Table S1 Peak positions of X-ray photoelectron and Auger electron spectra for S1–S3.

	C	N	S	Cu	Cu LMM	Ag	Ag MNN
S1 (eV)	284.6, 285.7, 286.6, 288.3	399.5, 401.5	161.9, 163.1	932.9, 952.7	575.5, 571.5, 568.9		
S2 (eV)	284.6, 285.5, 286.5, 288.2	399.8, 401.4	161.8, 163.0	932.7, 952.6	575.0, 571.6, 568.1	368.4, 374.4	1131.7, 1137.1
S3 (eV)	284.6, 285.6, 286.5, 288.2	399.8, 401.4	161.8, 163.1	932.8, 952.6	572.4, 568.1	368.5, 374.5	1131.8, 1137.3